RSC Advances

PAPER

View Article Online
View Journal | View Issue

Cite this: *RSC Adv.*, 2016, **6**, 53130

Influence of gold nanoparticles applied to catalytic hydrogenation of acetophenone with cationic complexes containing ruthenium†‡

Lanarck C. M. Souza,[a] Thiago A. Santos,[a] Cássio R. A. Do Prado,[a] Benedicto A. V. Lima,[b] Rodrigo S. Corrêa,§[b] Alzir A. Batista,[b] Larissa Otubo,[c] Javier Ellena,[d] Leonardo T. Ueno,[a] Luís R. Dinelli[a] and André L. Bogado*[a]

Received 2nd March 2016
Accepted 24th May 2016

DOI: 10.1039/c6ra05616d

www.rsc.org/advances

Herein the catalytic activity of cationic ruthenium(II) complexes $[Ru]^+$ is described in the presence of gold nanoparticles ($AuNPs^{n-}$) in the transfer hydrogenation of acetophenone, to produce phenylethanol. The catalytic activity of the complexes, with a general formula *cis*-$[RuCl(CH_3OH)(P-P)(N-N)]^+$ or *cis*-$[RuCl(CH_3OH)(P)_2(N-N)]^+$ {where: P = triphenylphosphine (PPh_3); P–P = 1,1-bis(diphenylphosphino) methane (dppm); 1,2-bis(diphenylphosphino)ethane (dppe); 1,3-bis(diphenylphosphino)propane (dppp), 1,4-bis(diphenylphosphino)butane (dppb); N–N = 2,2′-bipyridine; 4,4′-dimethyl-2,2′-bipyridine} was investigated in the presence of $AuNPs^{n-}$. The interaction between $[Ru]^+$ and $AuNPs^{n-}$ citrate capped is an electrostatic interaction, by a self-assembly processes, to produce a supramolecular species, labeled as $[Ru]^+/AuNPs^{n-}$. This non-covalent interaction has no effect over the chemical and physical chemical parameters of the complexes, which provides a good point of comparison in the presence and absence of $AuNPs^{n-}$. The $AuNPs^{n-}$ alone have no catalytic activity in the transfer hydrogenation of acetophenone within 24 h of reaction. However, the $AuNPs^{n-}$ have improved the catalytic activity of the complexes that have biphosphines with tensioned or large bite angle, while for the complexes that have biphosphines with a strong chelate effect a decrease in the catalytic activity was observed. The evidence is supported by experimental values of the yields of the hydrogenated product and DFT calculations of the "RuP–P" intermediates. Suitable crystals of *cis*-$[RuCl_2(dppe)(bipy)]$, *cis*-$[RuCl_2(dppp)(bipy)]$ and *cis*-$[RuCl(CH_3OH)(dppb)(bipy)](PF_6)$ were obtained and the X-ray structures are presented here.

Introduction

The use of complexes containing ruthenium in the hydrogenation of polar double bonds can occur by two main pathways: by hydrogenation or transfer hydrogenation.[1–3] One of the most important mechanisms for H_2-hydrogenation of imines and ketones was proposed by R. Noyori[4–7] (Nobel Prize laureate in 2001) and some insights were offered by R. H. Morris.[6,7] The most used catalyst precursors for this kind of reaction are complexes with phosphine and diamine moieties,[4–7] paying special attention to complexes containing ruthenium.[8–10]

Additionally, gold nanoparticles ($AuNPs^{n-}$), have been used in many areas of knowledge, for example: chemiluminescence sensors,[11] cross-link agents,[12] colorimetric detection,[13] modifier electrodes,[14,15] cytotoxicity studies,[16] hybrid nano-biomaterials,[17–19] biodiagnostics[20] and catalysis in liquid phases.[17–22] In agreement with the catalytic context, $AuNPs^{n-}$ have also been proposed as a key species in the water–gas-shift reaction (WGSR). This consists of a carboxyl mechanism for the WGSR on the $AuNPs^{n-}/CeO_2(111)$ surface, where the pathway for H_2 production recombines two H atoms to form H_2 on the Au cluster.[23–29] Catalytic activity of $Au_{25}(SR)_{18}$ nanoclusters (R = C_2H_4Ph) for the aldehyde hydrogenation reaction in the presence of a base has been reported by Kim and co-workers.[30] The ability of functionalized $AuNPs^{n-}$ in the reduction of 4-nitrophenol to produce 4-aminophenol is another interesting application of $AuNPs^{n-}$ in catalyses.[15,31–39]

[a]*Faculdade de Ciências Integradas do Pontal, Universidade Federal de Uberlândia, Rua vinte, 1600, CEP 38304-402, Ituiutaba, MG, Brazil. E-mail: bogado@ufu.br*

[b]*Departamento de Química, Universidade Federal de São Carlos, CP 676, CEP 13565-905, São Carlos, SP, Brazil*

[c]*Centro de Ciência e Tecnologia de Materiais, Instituto de Pesquisas Energéticas e Nucleares, Av. Prof. Lineu Prestes, 2242-Cidade Universitária, CEP: 05508-000, São Paulo, SP, Brazil*

[d]*Instituto de Física de São Carlos, Universidade de São Paulo, CP 780, 13560-970, São Carlos, SP, Brazil*

† In memoriam of Prof. Peter Hofmann (Organisch-Chemisches Institut, Ruprecht-Karls-Universität Heidelberg).

‡ Electronic supplementary information (ESI) available. CCDC 1457016, 1457017 and 1456936. For ESI and crystallographic data in CIF or other electronic format see DOI: 10.1039/c6ra05616d

§ Present address: Universidade Federal de Ouro Preto, Campos Morro do Cruzeiro, CEP 35.400-000 Ourto Preto – MG – Brasil.

Recently, we demonstrated that interaction between cationic ruthenium complexes and $AuNPs^{n-}$ does not change the structure and geometry of the complexes, neither the electronic properties of them.[12,14] These cationic ruthenium complexes are used as positive charge species in order to aggregate on the surface of negatively charged gold nanoparticles, by a self-assembly processes, which depends only on the concentration of the related species. The maintenance of chemical attributes of the complexes, after interacting with $AuNPs^{n-}$, provides an application of these new materials in different fields.

Herein the effect of $AuNPs^{n-}$ in the transfer hydrogenation of acetophenone catalyzed by cationic complexes containing ruthenium is described. Suitable crystals of *cis*-[$RuCl_2$(dppe)(bipy)], *cis*-[$RuCl_2$(dppp)(bipy)] and *cis*-[$RuCl(CH_3OH)$(dppb)(bipy)](PF_6) were obtained and the X-ray structures are presented here.

Results and discussion

Syntheses and characterization of complexes containing ruthenium

The ruthenium complexes were firstly synthesized as dichloride ruthenium complexes. The designation *cis* and *trans* are related to the chloride position in the structure of the complexes. The complexes with a general formula *cis*-[$RuCl_2$(P–P)(N–N)] {where: P–P = 1,4-bis(diphenylphosphino)butane (dppb), N–N = 2,2′-bipyridine (bipy) or 4,4′-dimethyl-2,2′-bipyridine (Meby)} where synthesized from the binuclear complex containing ruthenium [$RuCl_2$(dppb)]$_2$-μ-(dppb)[40,41] as described previously.[42–44] The *trans*-[$RuCl_2(PPh_3)_2$(bipy)] {where: PPh_3 = triphenylphosphine (PPh_3)} was prepared from the well-known complex containing ruthenium described by Wilkinson[45] [$RuCl_2(PPh_3)_3$].[42,43] The complexes *cis*-[$RuCl_2$(dppm)(bipy)], *cis*-[$RuCl_2$(dppe)(bipy)] and *cis*-[$RuCl_2$(dppp)(bipy)] were synthesized from the *trans*-[$RuCl_2$(bipy)(PPh_3)$_2$] by phosphine exchange. The $^{31}P\{^1H\}$ NMR spectra of *cis*-[$RuCl_2$(dppm)(bipy)], *cis*-[$RuCl_2$(dppe)(bipy)] and *cis*-[$RuCl_2$(dppp)(bipy)] show two doublets, which are in agreement with the non-magnetic equivalence of the P atoms, suggesting a *cis* coordination mode of the ligands. The chemical shift of these complexes show an inverse relationship with the Ru–P bond lengths, determined by single crystal X-ray diffraction, where the more shielded phosphorus atoms provide a longer Ru–P bond, and consequently a weaker bond. The anodic peak potential (E_{pa}) observed by cyclic voltammetry (CV) is in agreement with $^{31}P\{^1H\}$ NMR data and bond lengths for Ru–P. Thus, the higher value of E_{pa} was observed in the CV of the *cis*-[$RuCl_2$(dppe)(bipy)] (0.73 V), due to the stronger back-donation ruthenium to phosphorus, when compared with the same bond for the *cis*-[$RuCl_2$(dppp)(bipy)] (see Table 1).

The X-ray structures of *cis*-[$RuCl_2$(dppe)(bipy)] and *cis*-[$RuCl_2$(dppp)(bipy)] are shown in Fig. 1 and 2, respectively. Selected bond, distances and angles are available in the ESI.† The structures of *cis*-[$RuCl_2$(dppe)(bipy)] and *cis*-[$RuCl_2$-(dppp)(bipy)] are distorted octahedrally, due to the restricted bite angles of the surrounding bidentate ligands in the molecular structure of the complexes.

The biphosphine bite angle is shorter in the *cis*-[$RuCl_2$-(dppe)(bipy)], when compared with *cis*-[$RuCl_2$(dppp)(bipy)], P(2)–Ru–P(1) = 84.91(3)° and P(2)–Ru(1)–P(1) = 92.85(10)°, respectively. These results are in agreement with electrochemical and $^{31}P\{^1H\}$ NMR data. The bond distances and angles[47,48] of *cis*-[$RuCl_2$(dppe)(bipy)] and *cis*-[$RuCl_2$(dppp)(bipy)] complexes are in the range expected for biphosphine complexes containing ruthenium.[42–44]

The related cationic ruthenium solvate complexes [$RuCl(CH_3OH)$(dppb)(bipy)]$^+$ (**1**), [$RuCl(CH_3OH)$(dppb)(Mebipy)]$^+$ (**2**), [$RuCl(CH_3OH)(PPh_3)_2$(bipy)]$^+$ (**3**), [$RuCl(CH_3OH)$(dppm)(bipy)]$^+$ (**4**), [$RuCl(CH_3OH)$(dppe)(bipy)]$^+$ (**5**) and [$RuCl(CH_3OH)$(dppp)(bipy)]$^+$ (**6**), were prepared after adding the dichloro ruthenium complexes (10 μmol each), in methanol (2 mL), within 1 h of magnetic stirring at room temperature. The *cis* designation

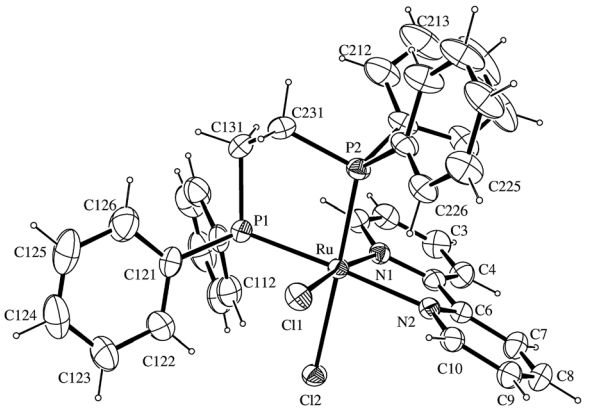

Fig. 1 ORTEP view[46] and atomic numbering of *cis*-[$RuCl_2$(dppe)(bipy)].[47]

Table 1 $^{31}P\{^1H\}$ NMR chemical shift and $E_{1/2}$ potentials of *cis*-[$RuCl_2$(dppm)(bipy)], *cis*-[$RuCl_2$(dppe)(bipy)] and *cis*-[$RuCl_2$(dppp)(bipy)]

Complex	δ^a ppm ($^2J_{PP}$ = Hz)	Ru–P bond lengths[b] (Å)	$E_{pa}{}^c$ (V) (Ru^{II}/Ru^{III})
Cis-[$RuCl_2$(dppm)(bipy)]	18.5; 11.2 (64.3)	—	0.68
Cis-[$RuCl_2$(dppe)(bipy)]	68.0; 61.0 (54.0)	Ru–P_2 (*trans* Cl) = 2.2465(8) Ru–P_1 (*trans* N_2) = 2.2907(9)	0.73
Cis-[$RuCl_2$(dppp)(bipy)]	40.2; 32.3 (42.1)	Ru–P_2 (*trans* Cl_{11}) = 2.280(3) Ru–P_1 (*trans* N_{12}) = 2.313(3)	0.69

[a] Using CH_2Cl_2 as a solvent (D_2O capillary), δ with respect to the phosphorus signal of H_3PO_4 85%. [b] Obtained by single crystal X-ray diffraction. [c] CV were carried out at room temperature in CH_2Cl_2 containing 0.1 mol L^{-1} $Bu_4N^+ClO_4^-$ (TBAP). The working and auxiliary electrodes consisted of stationary Pt foil; the reference electrode was Ag/AgCl in a Luggin capillary.

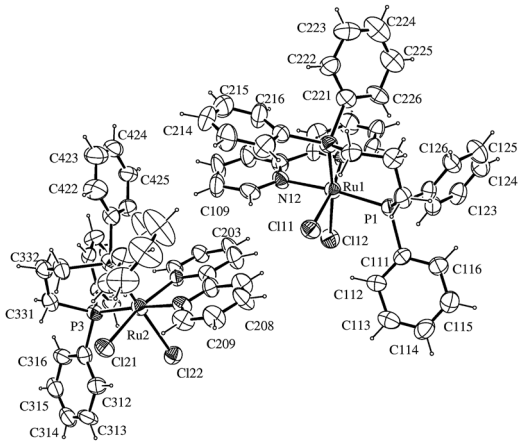

Fig. 2 ORTEP view[46] and atomic numbering of *cis*-[$RuCl_2$(dppp)(bipy)].[48]

in the chemical formulas of cationic complexes is related to the position of coordinated Cl and CH_3OH groups (see Scheme 1). Suitable crystals of *cis*-[$RuCl(CH_3OH)$(dppb)(bipy)](PF_6) grown by slow evaporation of diethyl methanol/CH_2Cl_2 and their structure was determined by single crystal X-ray diffraction (Fig. 3).

The structure of *cis*-[$RuCl(CH_3OH)$(dppb)(bipy)]$^+$ is also distorted octahedrally, with a methanol molecule coordinated in the *trans* position of P-atom. Experimental and theoretical study of the kinetics of dissociation in the *cis*-[$RuCl_2$(dppb)(bipy)] revealed that only the chloride *trans* to the phosphorus atom of the dppb ligand was dissociated, even in the presence of excess of monodentate ligand, such as monopyridine and functionalized monopyridine.[51]

Interaction between $[Ru]^+$ and $AuNPs^-$

Recently, we (and other authors) have demonstrated the non-covalent interaction between $AuNPs^{n-}$ and cationic specimens with different applications in many areas of knowledge.[12,14,52–54] The process of interaction between cationic ruthenium complexes $[Ru]^+$ and the negative surface of gold nanoparticles

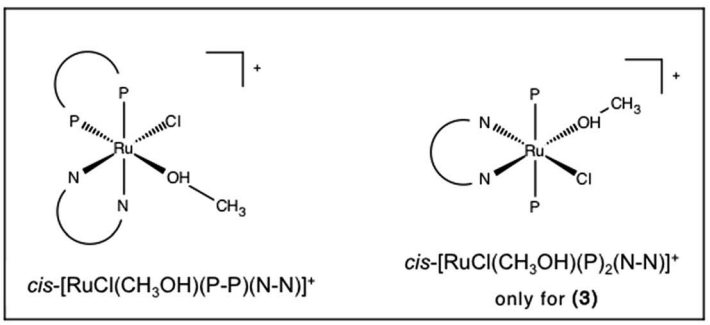

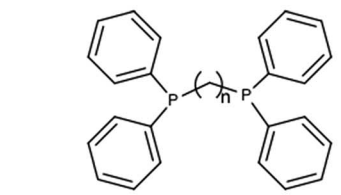

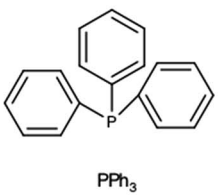

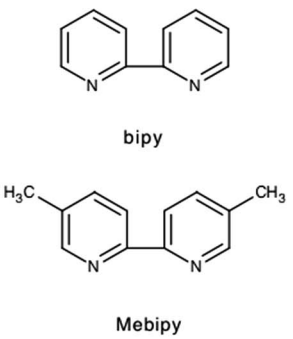

Complex	P - Donor Group	N - Donor Group
(1)	dppb	bipy
(2)	dppb	Mebipy
(3)	PPh_3	bipy
(4)	dppm	bipy
(5)	dppe	bipy
(6)	dppp	bipy

Scheme 1 General structures of complexes studied in this work as Cl^- salts.[50]

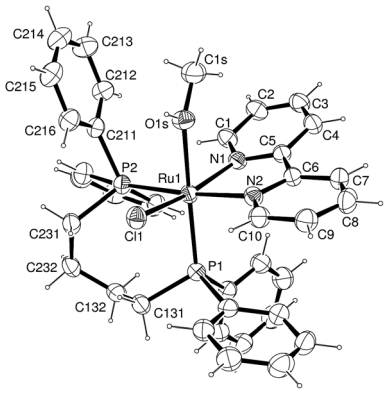

Fig. 3 ORTEP view[46] and atomic numbering of $[RuCl(dppb)(bipy)(CH_3OH)]^+$.[49]

($AuNPs^{n-}$) can be accompanied by optical measurements and TEM images. The plasmon band adsorption of $AuNPs^{n-}$ occurs at 520 nm, and the addition of $[Ru]^+$ specimens produce an enlarged band, centralized at 625 nm, with a significant decrease in the original plasmon band. The polarization of the conduction electron oscillations in adjacent $AuNPs^{n-}$ causes a red-shift on the plasmon absorbance, attributed to the coupling of plasmon absorbance of the particles.[55,56] The time dependence of the interaction between $[Ru]^+$ and $AuNPs^{n-}$ was carried out using optical measurements (UV/vis), with temperature control, using the cationic complex containing ruthenium with formula $[RuCl(py)(dppb)(bipy)]^+$ {where py = pyridine}.[12,14] Stock solutions of the cationic complexes were prepared in acetone (5.3×10^{-5} mol L^{-1}) and 100 μL of that was added to a colloidal suspension of $AuNPs^{n-}$ (3 mL, 0.05 mol L^{-1}). The kinetics of interaction between $AuNPs^{n-}$ with $[Ru]^+$ was investigated by monitoring the changes in the electronic spectra as a function of time and temperature in the range from 20 °C to 35 °C (Fig. 4).

Herein the terms used by Whitesides and co-workers,[57] are adopted. They use *flocculation* to refer to the instability of colloidal dispersions, *agglomeration* for the cases involving reversible association of nanoparticles and *aggregation* for irreversible association.

In Fig. 4, it can be observed that the induction and flocculation period (a and b) is dependent on the temperature range, and at 30 °C the flocculation period practically disappears, and the interaction between $AuNPs^{n-}$ and $[Ru]^+$ species go directly to the aggregation. Bellino and co-workers[58] investigated the kinetics of interaction of citrate stabilized gold nanoparticles with negatively and positively charged mercapto ligands. Another interesting aspect is the possibility of controlling the stabilization/destabilization of $AuNPs^{n-}$ with pentacyanoferrate(II) ions.[56] In both cases, the kinetics proceed relatively fast, leading to the decay of the 520 nm band and the rise of the plasmon coupling band at 650 nm, a characteristic of flocculation. In a typical experiment using the Arrhenius equation in its linear form, the logarithmic of kinetic constants, obtained by the initial rate method, were plotted against the inverse of temperature (Fig. 5).

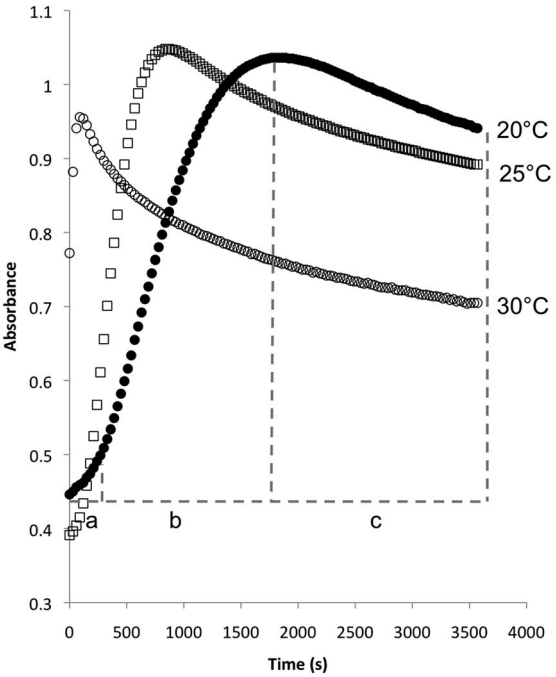

Fig. 4 Time dependence of coupled plasmon band of $AuNPs^{n-}$ (3 mL; 0.05 mol L^{-1}) in the presence of $[RuCl(py)(dppb)(bipy)]^+$ (100 μL, 5.3×10^{-5} mol L^{-1}) as a function of time $\lambda = 625$ nm; temperature: 20, 25 and 30 °C. The label inside 20 °C UV/vis: a = induction time, b = flocculation ($t = 25$ min), c = aggregation.

The activation energy (E_a) and the pre-exponential factor (A) were obtained related to flocculation and aggregation period (Table 2). The E_a of the flocculation period is 46.14 kJ mol^{-1}, which is higher than the E_a of the aggregation period, 38.88 kJ mol^{-1}. It is reasonable that the E_a to promote a flocculation should be higher than the E_a to promote an aggregation, since the species should meet each other, with appropriate kinetic energy to produce an aggregate. The pre-exponential factor is also in conformity, the A value of the flocculation period is almost one thousand times higher than the aggregation period.

TEM images of the flocculation period were obtained, where the $[RuCl(py)(dppb)(bipy)]^+$ (0–1000 μL, 5.3×10^{-5} mol L^{-1} in acetone) was added to a colloidal suspension of $AuNPs^{n-}$ (1.0 mL, 0.05 mol L^{-1}) (Fig. 6). The TEM images show an average diameter of the $AuNPs^{n-}$ of approximately 12 nm and reveal that they did not grow in a radial mode when the $[Ru]^+$ species are present, but in the flocculation period, the approximation of the spherical nanoparticles is observed. It is in agreement with the optical measurements observed by UV/vis, with the appearance of the coupled plasmon band at 625 nm. A precipitate is formed in the presence of a large excess of the $[Ru]^+$, labeled as an assembly of $AuNPs^{n-}$ and the $[Ru]^+$ ($[Ru]^+$/$AuNPs^{n-}$), and it is observed as round-shaped bright spots, which is soluble in 2-propanol, as previously published.[12,14]

Catalytic activity of the complexes and DFT calculation

It can be observed in the Table 3 that $AuNPs^{n-}$ has no catalytic activity in the hydrogenation of acetophenone, with the applied

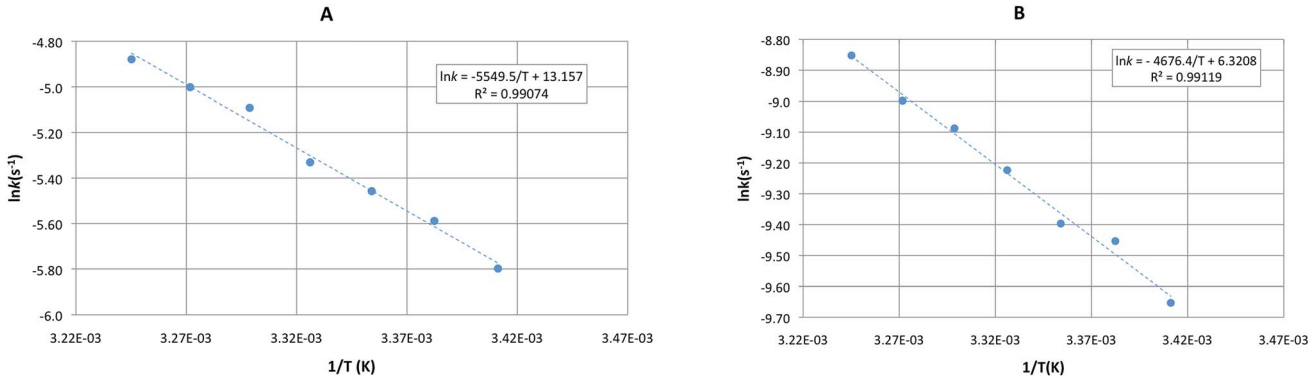

Fig. 5 Arrhenius plot. (A) Flocculation period. (B) Aggregation period.

Table 2 Kinetic parameters obtained from Arrhenius plot of coupled plasmon band of AuNPs^{n-} promoted by [RuCl(py)(dppb)(bipy)]$^{+}$

Coupled plasmon band at $\lambda = 625$ nm	E_a (kJ mol^{-1})	ln A	A
Flocculation period	46.14	13.157	517 621
Aggregation period	38.88	6.32	556

conditions, within 5.5 h of reaction. However, it can improve the catalytic activity of some biphosphine complexes containing ruthenium, within 1 h of reaction. When the (**1**)/AuNPs^{n-} was used as a pre-catalyst, it produced 24% more phenylethanol than (**1**) alone. The time dependence of (**1**)/AuNPs^{n-} showed that the quantitative amount of product can be obtained after 2 h of reaction, and the best molar relationship between (**1**) and AuNPs^{n-} was 2.0/1.0 respectively, as described in the caption in Table 3. When the (**2**)/AuNPs^{n-} was used as a pre-catalyst, it produced almost 12% more product. There is no significant improvement when (**3**) was used as a pre-catalyst. In this case, in the presence or absence of AuNPs^{n-}, the amount of formed product is almost the same, with an average of 81.69% of product. When the (**3**)/AuNPs^{n-} was used as a pre-catalyst, with an additional amount of PPh_3 (5 eq. in respect of the ruthenium complex), a drastic decrease in the catalytic activity was observed, only 3% of the product was observed after 24 h of reaction. In the first moment, it suggests that an intermediate species with an uncoordinated phosphine, or a dangling biphosphine, could be the real catalyst of that reaction, and the AuNPs^{n-} could be acting as a co-catalyst in the transfer hydrogen pathway from isopropanol to substrate.

To better understand this behavior, the ΔG° energy to produce a dangling biphosphine was determined by DFT calculation (see Scheme 2). The values of ΔG° are described in the Scheme 2, with positive values of ΔG° in all cases, which suggest that dissociation of one side of P–P is a non-spontaneous process. On the other hand, the coordination κ^2-P–P mode is a spontaneous process.

In Fig. 7, it can be observed that the catalytic activity tendency, without AuNPs^{n-}, follows the thermodynamic stability of the applied complexes containing ruthenium, due to the structure of a dangling biphosphine. However, the tendency is opposite when AuNPs^{n-} is applied to the catalytic system. The catalytic activity of the precursors (**5**) and (**6**) decrease in the presence of AuNPs^{n-}, which has support in the thermodynamic stability of the complexes. As they have a higher stability, the interaction with AuNPs^{n-} should be more effective, therefore the catalytic performance decreases. For the sake of illustration, the precursor (**5**) exhibits the higher ΔG° value among the studied precursors, with 108.3 kJ mol^{-1} due to the η^1-P–P coordination mode. This suggests that (**5**) is a stable complex, as expected by the coordination chemistry knowledge, and it showed the best catalytic activity without AuNPs^{n-}, with 93% of the phenylethanol after 1 h of reaction.

More outstanding results were obtained from precursors (**1**) and (**4**) in the presence of AuNPs^{n-}, suggesting that these nanoparticles can improve the catalytic activity of the complexes that have biphosphines with tensioned or large bite

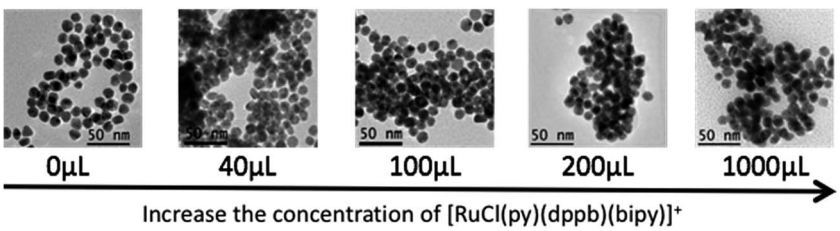

Fig. 6 TEM images of the flocculation period between a colloidal suspension of AuNPs^{n-} (0.05 mol L^{-1}) and [RuCl(py)(dppb)(bipy)]$^{+}$ (0–1000 μL), 5.3×10^{-5} mol L^{-1} in acetone.

Table 3 Transfer hydrogenation of acetophenone with $[Ru]^+/AuNPs^{n-a}$

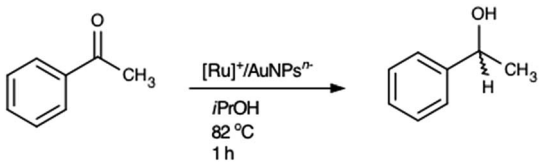

	Phenylethanol%		TOF (h^{-1})	
Pre-catalyst	Without $AuNPs^{n-}$	With $AuNPs^{n-}$	Without $AuNPs^{n-}$	With $AuNPs^{n-}$
$AuNPs^{n-(a)}$	—	4.01	—	—
(**1**)	48.75	77.74	487	777
(**2**)	72.95	84.40	729	875
(**3**)	87.48	75.90	875	759
(**4**)	24.10	71.23	240	710
(**5**)	93.54	24.20	930	240
(**6**)	50.53	35.94	500	350
(**3**) + 5 eq. PPh_3 [(b)]	—	3.00	—	—

[a] Applied ruthenium complexes $[RuCl(CH_3OH)(dppb)(bipy)]^+$ (**1**); $[RuCl(CH_3OH)(dppb)(Mebipy)]^+$ (**2**); $[RuCl(CH_3OH)(PPh_3)_2(bipy)]^+$ (**3**); $[RuCl(CH_3OH)(dppm)(bipy)]^+$ (**4**); $[RuCl(CH_3OH)(dppe)(bipy)]^+$ (**5**); $[RuCl(CH_3OH)(dppp)(bipy)]^+$ (**6**). Every reaction was carried out in threefold analysis. TOF = turnover frequency = mol phenylethanol/mol $[Ru]^+$/h. Time = 1 h, except in (a) t = 5.5 h, and (b) t = 24 h. $AuNPs^{n-}$ = 10 mL (0.05 mol L^{-1}). Molar relationship $[Ru]^+/AuNPs^{n-}$/acetophenone/KOH = 1/0.5/1000/20.

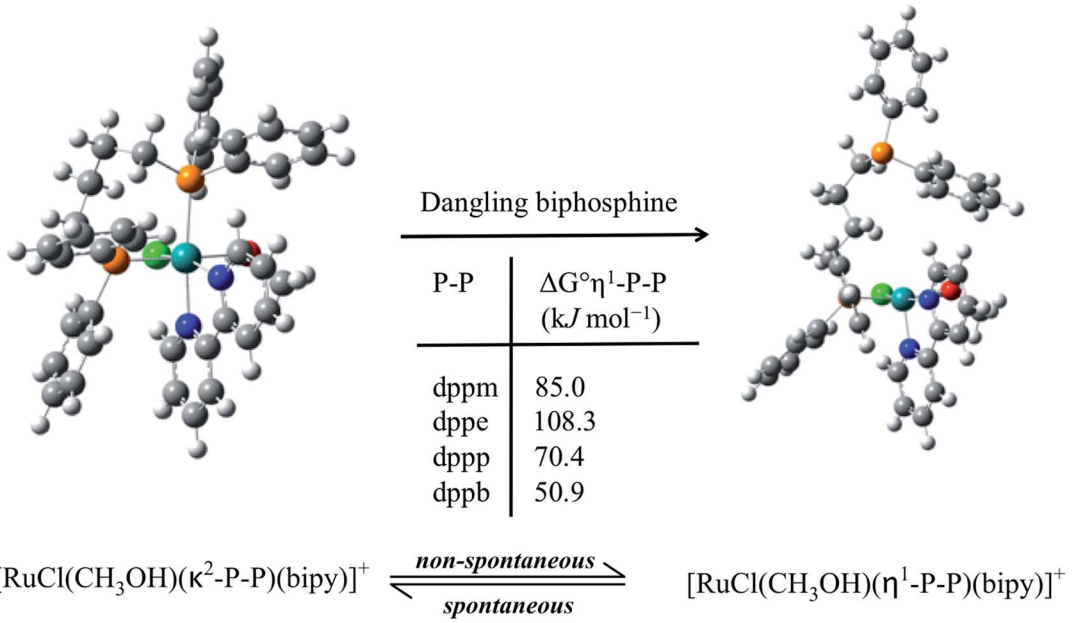

Scheme 2 Thermodynamic stability of the complexes $[RuCl(CH_3OH)(dppb)(bipy)]^+$ (**1**), $[RuCl(CH_3OH)(dppm)(bipy)]^+$ (**4**), $[RuCl(CH_3OH)(dppe)(bipy)]^+$ (**5**) and $[RuCl(CH_3OH)(dppp)(bipy)]^+$ (**6**) due to the dissociation of one side of P–P.

angle. In some way, the $AuNPs^{n-}$ can stabilize the structure of these complexes, strongly suggested by η^1-P–P type coordination. Thus, these reaction intermediates can act as effective catalyst precursors. Therefore, there seem to be two different pathways acting in the catalytic systems of those complexes: one related to dppe and dppp, and the other to dppm and dppb complexes containing ruthenium.

The Cl^- dissociation was also investigated by DFT in the complexes with general formula $[RuCl(CH_3OH)(\kappa^2\text{-P–P})(bipy)]^+$, and the energy to produce the dicationic complexes was surprisingly over 800 kJ mol^{-1}. It suggests that the real catalyst should keep at least one anionic ligand coordinated in the metal centre, which could be the Cl^-, or a hydride species formed *in situ*.

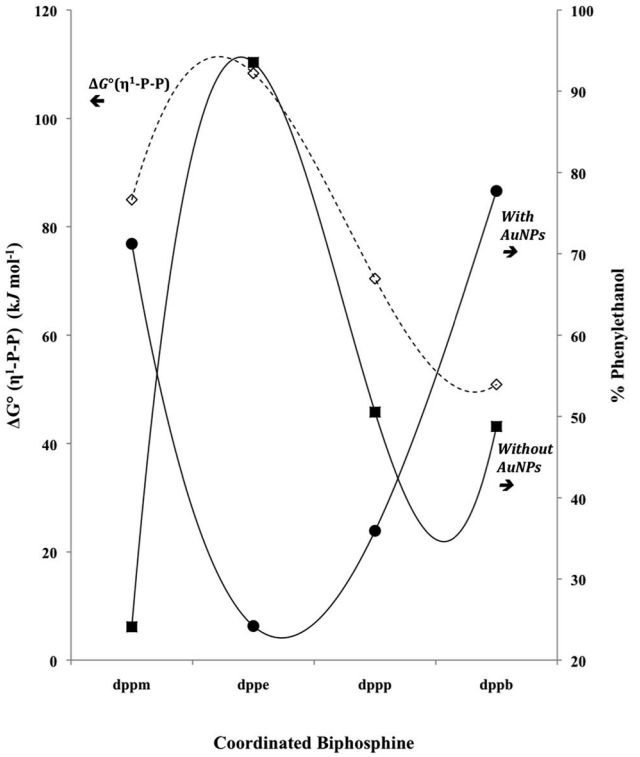

Fig. 7 Relationship between standard free-Gibbs energies for one site dissociation of P–P ligand (dashed line) and amount of catalytic product (solid lines: ■ = without AuNPs^{n-}, ● = with AuNPs^{n-}).

The dependence of the product on the P–P ligand was also observed in the reactions of $[RuCl_3(NO)(P–P)]$ complexes with 2-mercaptopyridine (pyS) ligand.[59] When the P–P ligand was dppen {1,2-bis(diphenylphosphino)ethylene}, dppe or dppp, the only product was the corresponding $[Ru(pyS)_2(P–P)]$ complexes. However, with dppm and dppb a different pattern of reactivity was found and the main product was identified as $[Ru(pyS)_2(NO)(\eta^1\text{-P–PO})]PF_6$.

Experimental

Reagents

All reactions were carried out under an argon atmosphere using standard Schlenk techniques. $RuCl_3 \cdot xH_2O$, $H[AuCl_4]$, triphenylphosphine (PPh_3), 1,1-bis(diphenylphosphino)methane (dppm), 1,2-bis(diphenylphosphino)ethane (dppe), 1,3-bis(diphenylphosphino)propane (dppp), 1,4-bis(diphenylphosphino) butane (dppb), 2,2′-bipyridine (bipy), 4,4′-dimethyl-2,2′-bipyridine (Mebipy), pyridine (py), 4′-methylpyridine (Mepy), 4′-*tert*-butylpyridine (*t*but-py), 4′-vinylpyridine and sodium citrate were purchased from Aldrich and used as received. Reagent grade solvents were distilled prior to use.

Instrumentation

Ruthenium complexes were analyzed by $^{31}P\{^1H\}$ NMR on an ARX 200 MHz and a DRX 400 MHz Bruker instrument. Samples were prepared under an inert atmosphere of argon and analyzed at room temperature with a D_2O capillary and dichloromethane (CH_2Cl_2) as solvent. Chemical shifts are relative to the signal of H_3PO_4, 85%, as an external reference. Cyclic voltammetry experiments were carried out at 25 °C in CH_2Cl_2 containing 0.1 mol L^{-1} $Bu_4N^+ClO_4^-$ (TBAP), with a Bioanalytical System Inc. BAS-100B/W electrochemical analyzer. The working and auxiliary electrodes were stationary Pt foil; a Luggin capillary probe was used and the reference electrode was Ag/AgCl. Under the conditions used, E^0 for the one-electron oxidation of $[Fe(\eta^5\text{-}C_5H_5)_2]$, added to the test solutions as an internal reference, is +0.43 V. Elemental analyses were performed at the Department of Chemistry at the Federal University of São Carlos, (Brazil), with a FISIONS CHNS EA1108 micro analyzer. Suitable crystals for X-ray analyses were grown by slow evaporation of a dichloromethane-diethyl ether solution of *cis*-$[RuCl_2(dppe)(bipy)]$, *cis*-$[RuCl_2(dppp)(bipy)]$ and *cis*-$[RuCl(CH_3OH)(dppb)(bipy)](PF_6)$.

The syntheses of gold nanoparticles and the aggregation with cationic ruthenium complexes were controlled by UV/vis analyses on a Shimadzu UV spectrophotometer model UV-1800 with a Shimadzu temperature controlled cell hold model TCC-100.

Transmission electron microscopy (TEM) images were obtained using a JEOL JEM 2100 operating at 200 kV. The sample was prepared as follows: stock solutions of the cationic complexes were prepared in acetone (5.3×10^{-5} mol L^{-1}) and 100 μL of this was added to a colloidal suspension of AuNPs^{n-} (3 mL, 0.05 mol L^{-1}). The resulting solution was dropped onto a 400 mesh copper grid coated with collodion film.

All calculations were carried out using the Gaussian09 suite of programs.[60] The structures were optimized by the Density Functional Theory (DFT) method, using the B3LYP hybrid functional, which includes the non-local exchange term with three parameters of Becke and the correlation term of Lee–Yang–Parr.[61,62] The basis set used to build the molecular orbitals were the Los Alamos effective core potential (ECP) and double-zeta valence basis set (LanL2DZ) for ruthenium and 6-311+G(d,p) for the remaining atoms. The Hessian matrix was calculated for the optimized structures in order to verify the nature of the stationary state.

X-ray diffraction data

The crystals were mounted on an Enraf-Nonius Kappa-CCD diffractometer with graphite monochromated MoKα (λ = 0.71073 Å) radiation. The final unit cell parameters were based on all reflections. Data collections for all complexes were carried out at room temperature (293 K), with the COLLECT program;[63] integration and scaling of the reflections were performed with the HKL Denzo–Scalepack system of programs.[64] The crystal structures were solved by the direct method using SHELXS-97 (ref. 65) and refined anisotropically (non-hydrogen atoms) by full-matrix least-squares on F^2 using a SHELXL-97 (ref. 65) program. A Gaussian method implemented was used for the absorption corrections.[66] All hydrogen atoms were positioned stereochemically and refined using the riding model. The program ORTEP-3 (ref. 46) was used to draw the molecules. Table 1, in

the ESI,† summarizes the data collection and experimental details of *cis*-[$RuCl_2$(dppe)(bipy)], *cis*-[$RuCl_2$(dppp)(bipy)] and *cis*-[RuCl(CH_3OH)(dppb)(bipy)](PF_6).

Preparation of gold nanoparticles ($AuNPs^{n-}$)

$AuNPs^{n-}$ with a diameter of 10–18 nm were prepared by citrate reduction of $H[AuCl]_4$ in aqueous solution according to a well-known method described by Frens.[67] To summarize, 20 μL of solution containing $H[AuCl]_4$ (Au 58%) was added to 100 mL of water. The resulting solution was brought to reflux, and 3 mL of sodium citrate solution (1%) was introduced while stirring. The solution was then kept boiling for another 30 min, while the colors changed from yellow to deep blue to red. Finally, the solution was left to cool to room temperature.

Synthesis of ruthenium complexes

***Cis*-[$RuCl_2$(dppp)(bipy)].** In a Schlenk tube, the *trans*-[$RuCl_2$(bipy)(PPh_3)$_2$][42] (428 mg, 0.502 mmol) was dissolved in CH_2Cl_2 (20 mL), and dppp (255 mg, 0.618 mmol) was added. After 30 min of reflux, the color of the solution changed from yellow to deep red, and a fine powder was observed, which was filtered off by cannula filtration. The remained solution was refluxed for 30 min more and the volume was reduced to approximately 5 mL. The product was precipitated with diethyl ether (10 mL). The obtained solid was filtered off, washed with diethyl ether (3 × 5 mL) and dried under vacuum. Yield: 85%. Anal. calcd for $C_{37}H_{34}Cl_2N_2P_2Ru$: exptl (calc): C, 60.31 (60.01); N, 3.83 (3.78); H, 4.72 (4.66). $^{31}P\{^1H\}$ (CH_2Cl_2/D_2O) δ: 40.2 and 32.3 ppm (d, $^2J_{PP} = 42.1$ Hz). FTIR (KBr): Ru–Cl 273 and 318 cm^{-1} (w) VC: E_{pa} = 690 mV, $E_{1/2}$ = 648 mV, $|I_{pa}/I_{pc}|$ = 0.92. Suitable crystals were grown by slow evaporation of diethyl ether/CH_2Cl_2 solution and the X-ray structure of *cis*-[$RuCl_2$(dppp)(bipy)] was determined.

***Cis*-[$RuCl_2$(dppe)(bipy)].** This synthesis was firstly described by Popov and co-workers.[68] However the synthesis was slightly changed and the related complex was obtained such as *cis*-[$RuCl_2$(dppe)(bipy)]. Herein, unpublished results about *cis*-[$RuCl_2$(dppe)(bipy)] will be discussed. Yield: 83%. Anal. calcd for $C_{36}H_{32}Cl_2N_2P_2Ru$: exptl (calc): C, 59.78 (59.52); N, 3.86 (3.86); H, 4.50 (4.44). $^{31}P\{^1H\}$ (CH_2Cl_2/D_2O) δ: 68.0 and 61.0 ppm (d, $^2J_{PP} = 54.0$ Hz). FTIR (KBr): Ru–Cl 268 and 308 cm^{-1}. VC: E_{pa} = 726 mV, $E_{1/2}$ = 661 mV, $|I_{pa}/I_{pc}|$ = 0.98. Suitable crystals were grown by slow evaporation of diethyl ether/CH_2Cl_2 solution and the X-ray structure of *cis*-[$RuCl_2$(dppe)(bipy)] was determined.

***Cis*-[$RuCl_2$(dppm)(bipy)].** This synthesis was carried out in a dark room to avoid the isomerization of the *cis* form to the *trans* of this complex. In a Schlenk tube the *trans*-[$RuCl_2$-(bipy)(PPh_3)$_2$][42] (428 mg, 0.502 mmol) was dissolved in CH_2Cl_2 (20 mL), and dppm (255 mg, 0.618 mmol) was added. After 30 min of reflux a fine powder was observed, which was filtered off by cannula filtration. The remaining solution was refluxed for 30 min more and the volume of the solution was reduced to approximately 5 mL, and a solid was precipitated with diethyl ether (10 mL). The obtained solid was filtered off, washed with diethyl ether (3 × 5 mL) and dried under vacuum. Yield: 88%. Anal. calcd for $C_{35}H_{30}Cl_2N_2P_2Ru$: exptl (calc): C, 58.82 (59.00); N, 3.70 (3.93); H, 4.19 (4.24). $^{31}P\{^1H\}$ (CH_2Cl_2/D_2O) δ: 18.5 and 11.2 ppm ($^2J_{PP} = 64.3$ Hz). FTIR (KBr): Ru–Cl, 272 and 314 cm^{-1}. VC: E_{pa} = 680 mV, $E_{1/2}$ = 600 mV, $|I_{pa}/I_{pc}|$ = 1.06.

Kinetic measurements

The kinetics of interaction between $AuNPs^{n-}$ and $[Ru]^+$ was investigated by monitoring the changes in the electronic spectra as a function of time and temperature in the range from 20 °C to 35 °C. In a typical experiment using $[RuCl(py)(dppb)(bipy)]^+$, the complex is described as follow: a stock solution of the cationic complex was prepared in acetone (5.3×10^{-5} mol L^{-1}) and 100 μL of that was added to a colloidal suspension of $AuNPs^{n-}$ (3 mL, 0.05 mol L^{-1}). The time dependence of coupled plasmon band of $AuNPs^{n-}$ was recorded at $\lambda = 625$ nm by UV/vis analyses on a Shimadzu UV spectrophotometer model UV-1800 with a Shimadzu temperature controlled cell hold model TCC-100.

$[Ru]^+/AuNPs^{n-}$ preparation and catalyses

The dichloride ruthenium complexes were stirred for 1 hour in methanol, and after that, a colloidal suspension of $AuNPs^{n-}$ (10 mL, 0.05 mol L^{-1}) was added, and the resulting mixture was magnetically stirred for 10 min. The solvent was evaporated until dry, under vacuum, and the obtained solid, labeled as $[Ru]^+/AuNPs^{n-}$, was characterized as a supramolecular species, as described previously.[12,14] The $[Ru]^+/AuNPs^{n-}$ were applied to the transfer hydrogenation reaction of acetophenone, and a typical catalytic experiment is described as follows: the $[Ru]^+/AuNPs^{n-}$ was dissolved in 2-propanol (10 mL), and acetophenone (10 mmol, 0.2 mol L^{-1}) was added, in the presence of KOH (0.2 mol L^{-1} in 2-propanol). The catalytic reactions were carried out in argon atmosphere at 82 °C. Molar relationship $[Ru]^+/AuNPs^{n-}$/acetophenone/KOH = 1/0.5/1000/20. The reaction products were analyzed by gas chromatography using a Thermo Scientific GC – Focus chromatograph equipped with a FID detector. A LM-120 column (poly(ethyleneglycol), 25 m long, 0.25 mm i.d. 0.25 μm film thickness) was used to characterize acetophenone and phenylethanol. Hexadecane was used as an internal standard and N_2 was the gas carrier (2.0 mL min^{-1}). The temperature program was from 170 °C (2 min) to 200 °C (2 min) at a heating rate of 10 °C min^{-1}.

Conclusions

The interaction between $[Ru]^+$ and $AuNPs^{n-}$ citrate capped is an electrostatic interaction, by self-assembly processes, to produce a supramolecular species, labeled as $[Ru]^+/AuNPs^-$. The time dependence of the interaction between $[Ru]^+$ and $AuNPs^{n-}$ was investigated by optical measurements (UV/vis), with three different steps in solution: induction, flocculation and aggregation periods. All of these three steps are dependent on the temperature range; at 30 °C the flocculation period practically disappeared, and the interaction between $AuNPs^{n-}$ and $[Ru]^+$ specimens go directly to the aggregation. The Arrhenius parameters of the coupled plasmon band at $\lambda = 625$ nm reveal that the flocculation period is energetically higher than the aggregation period, and TEM images reveal that the $AuNPs^{n-}$

did not grow in a radial mode when the $[Ru]^+$ species were present. It provides only the approximation of the spherical nanoparticles, which are in agreement with the coupled plasmon band in the flocculation period observed by UV/vis. Therefore, the kinetic energy acquired in the flocculation period promotes the meeting of $[Ru]^+$ and $AuNPs^{n-}$, and it has enough energy to promote the aggregation of the specimens in solution, with a decrease in the *A* value.

This non-covalent interaction has no effect over the chemical and physical chemical parameters of the complexes, which provide a good point of comparison in the presence and absence of $AuNPs^{n-}$, when these species are applied to catalysis. The $AuNPs^{n-}$ alone has no catalytic activity in the transfer hydrogenation of acetophenone within 24 h of reaction. However, the $AuNPs^{n-}$ improved the catalytic activity of the complexes that have biphosphines with a tensioned or large bite angle, while the complexes that have biphosphines with a strong chelate effect, a decrease in the catalytic activity was observed. The evidence is supported by experimental values of the yields of the hydrogenated product and DFT calculation of the "RuP–P" intermediates. In general, complexes with lower values of $\Delta G^{\circ}_{\eta^1\text{-P-P}}$ are less stable in their chelate mode, and therefore these complexes showed a decrease in the catalytic activity, however in the presence of $AuNPs^{n-}$, the inverse behavior was observed.

Acknowledgements

We would like to thank FAPEMIG, CNPq, CAPES, FAPESP, FINEP, DAAD, and RQ-MG for their financial support. The authors are also thankful to the Grupo de Materiais Inorgânicos do Triângulo (GMIT) research group supported by FAPEMIG.

Notes and references

1 C. Elschenbroich, *Organometallics*, Wiley-VCH, Weinheim, 3rd edn, 2006.
2 D. Steinborn, *Fundamentals of Organometallic Catalysis*, Wiley-VCH, Weinheim, 1st edn, 2012.
3 R. H. Crabtree, *The Organometallic Chemistry of the Transition Metals*, John Wiley & Sons, New Jersey, 4th edn, 2005.
4 R. Noyori and H. Takaya, *Acc. Chem. Res.*, 1990, **23**, 345.
5 R. Noyori and T. Ohkuma, *Angew. Chem., Int. Ed.*, 2001, **40**, 40.
6 K. Abdur-Rashid, A. J. Lough and R. H. Morris, *Organometallics*, 2001, **20**, 1047.
7 K. Abdur-Rashid, S. E. Clapham, A. Hadzovic, J. N. Harvey, A. J. Lough and R. H. Morris, *J. Am. Chem. Soc.*, 2002, **50**, 15104.
8 M. P. de Araujo, A. T. de Figueiredo, A. L. Bogado, G. von Poelhsitz, J. Ellena, E. E. Castellano, C. L. Donnici, J. V. Comasseto and A. A. Batista, *Organometallics*, 2005, **24**, 6159.
9 T. F. Gallati, A. L. Bogado, G. von Poelhsitz, J. Ellena, E. E. Castellano, A. A. Batista and M. P. de Araujo, *J. Organomet. Chem.*, 2007, **692**, 5447.
10 D. A. Cavarzan, F. D. Fagundes, O. Fuganti, C. W. P. da Silva, C. B. Pinheiro, D. F. Back, A. Barison, A. L. Bogado and M. P. de Araujo, *Polyhedron*, 2013, **62**, 75.
11 E. Rampazzo, S. Bonacchi, D. Genovese, R. Juris, M. Marcaccio, M. Montalti, F. Paolucci, M. Sgarzi, G. Valenti, N. Zaccheroni and L. Prodi, *Coord. Chem. Rev.*, 2012, **256**, 1664.
12 V. F. Ferreira, C. R. A. do Prado, C. M. Rodrigues, L. Otubo, A. A. Batista, J. W. da Cruz Jr, J. Ellena, L. R. Dinelli and A. L. Bogado, *Polyhedron*, 2014, **78**, 46.
13 R. Manjumeena, D. Duraibabu, T. Rajamuthuramalingam, R. Venkatesan and T. Kalaichelvan, *RSC Adv.*, 2015, **5**, 69124.
14 K. M. de Oliveira, T. C. C. dos Santos, L. R. Dinelli, J. Z. Marinho, R. C. Lima and A. L. Bogado, *Polyhedron*, 2013, **50**, 410.
15 A. Ahmad, Y. wei, F. Syed, M. Imran, Z. U. H. Khan, K. Tahir, A. U. Khan, M. Raza, Q. Khan and Q. Yuan, *RSC Adv.*, 2015, **5**, 99364.
16 F. J. Osonga, I. Yazgan, V. Kariuki, D. Luther, A. Jimenez, P. Le and O. A. Sadik, *RSC Adv.*, 2016, **6**, 2302.
17 M.-C. Daniel and D. Astruc, *Chem. Rev.*, 2004, **104**, 293.
18 C. M. Niemeyer, *Angew. Chem., Int. Ed.*, 2001, **40**, 4128.
19 E. Katz and I. Willner, *Angew. Chem., Int. Ed.*, 2004, **43**, 6042.
20 N. L. Rosi and C. A. Mirkin, Nanostructures in Biodiagnostics, *Chem. Rev.*, 2005, **105**, 1547.
21 N. Yan, C. Xiao and Y. Kou, *Coord. Chem. Rev.*, 2010, **254**, 1179.
22 L. Liu, Y. Zhao, Q. Chen, X. Shi and M. Shen, *RSC Adv.*, 2015, **5**, 104239.
23 Y. Chen, H. Wang, R. Burch, C. Hardacre and P. Hu, *Faraday Discuss.*, 2011, **152**, 121.
24 L. C. Grabow, A. A. Gokhale, S. T. Evans, J. A. Dumesic and M. Mavrikakis, *J. Phys. Chem. C*, 2008, **112**, 4608.
25 A. A. Gokhale, J. A. Dumesic and M. Mavrikakis, *J. Am. Chem. Soc.*, 2008, **130**, 1402.
26 Z. P. Liu, S. J. Jenkins and D. A. King, *Phys. Rev. Lett.*, 2005, **94**, 196102.
27 J. A. Rodriguez, P. Liu, J. Hrbek, J. Evans and M. Perez, *Angew. Chem., Int. Ed.*, 2007, **46**, 1329.
28 X. M. Liu, Z. M. Ni, P. Yao, Q. Xu, J. H. Mao and Q. Q. Wang, *Acta Phys.–Chim. Sin.*, 2010, **26**, 1599.
29 L. Barrio, P. Liu, J. A. Rodriguez, J. M. Campos-Martin and J. L. G. Fierro, *J. Chem. Phys.*, 2006, **125**, 164715.
30 G. Li, H. Adroshan, Y. Chen, R. Jin and H. J. Kim, *J. Am. Chem. Soc.*, 2015, **137**, 14295.
31 N. Li, P. Zhao, M. E. Igartua, A. Rapakousiou, L. Salmon, S. Moya, J. Ruiz and D. Astruc, *Inorg. Chem.*, 2014, **53**, 11802.
32 N. Pradhan, A. Pal and T. Pal, *Colloids Surf., A*, 2002, **196**, 247.
33 A. Shivhare, S. J. Ambrose, H. Zhang, R. W. Purves and R. W. J. Scott, *Chem. Commun.*, 2013, **49**, 276.
34 P. Hervés, M. Pérez-Lorenzo, L. M. Liz-Marzán, J. Dzubiella, Y. Lu and M. Ballauff, *Chem. Soc. Rev.*, 2012, **41**, 5577.
35 P. Pachfule, S. Kandambeth, D. D. Díaz and R. Banerjee, *Chem. Commun.*, 2014, **50**, 3169.
36 Y. Zhang, X. Cui, F. Shi and Y. Deng, *Chem. Rev.*, 2012, **112**, 2467.

37 S. Wunder, Y. Lu, M. Albrecht and M. Ballauff, *ACS Catal.*, 2011, **1**, 908.
38 N. Pradhan, A. Pal and T. Pal, *Langmuir*, 2001, **17**, 1800.
39 K. Esumi, R. Isono and T. Yoshimura, *Langmuir*, 2004, **20**, 237.
40 M. Bressan and P. Rigo, *Inorg. Chem.*, 1975, **14**, 2286.
41 C. W. Jung, P. E. Garrou, P. R. Hoffman and K. G. Caulton, *Inorg. Chem.*, 1984, **23**, 726.
42 A. A. Batista, M. O. Santiago, C. L. Donnici, I. S. Moreira, P. C. Healy, S. L. Berners-Price and S. L. Queiroz, *Polyhedron*, 2001, **20**, 2123.
43 A. A. Batista, E. A. Polato, S. L. Queiroz, O. R. Nascimento, B. R. James and S. J. Rettig, *Inorg. Chim. Acta*, 1995, **230**, 111.
44 S. L. Queiroz, A. A. Batista, G. Oliva, M. T. do P. Gambardella, R. H. A. Santos, K. S. MacFarlane, S. J. Rettig and B. R. James, *Inorg. Chim. Acta*, 1998, **267**, 209.
45 T. A. Stepheson and G. Wilkinson, *J. Inorg. Nucl. Chem.*, 1966, **28**, 945.
46 L. J. Farrugia, ORTEP3 for Windows, *J. Appl. Crystallogr.*, 1997, **30**, 565.
47 Selected bond lengths and angles of *cis*-[$RuCl_2$(dppe)(bipy)] showing the atom labeling and 50% probability ellipsoids. Bond lengths (Å): Ru–N(1) 2.070(3), Ru–N(2) 2.129(3), Ru–P(2) 2.2465(8), Ru–P(1) 2.2907(9), Ru–Cl(1) 2.4267(9), Ru–Cl(2) 2.4815(8). Bond angles (°): N(1)–Ru–N(2) 77.75(10), N(1)–Ru–P(2) 92.67(7), N(2)–Ru–P(2) 98.99(7), N(1)–Ru–P(1) 99.21(8), N(2)–Ru–P(1) 175.11(7), P(2)–Ru–P(1) 84.91(3), N(1)–Ru–Cl(1) 172.10(8), N(2)–Ru–Cl(1) 94.42(8), P(2)–Ru–Cl(1) 89.62(3), P(1)–Ru–Cl(1) 88.52(4), N(1)–Ru–Cl(2) 88.91(7), N(2)–Ru–Cl(2) 81.90(7), P(2)–Ru–Cl(2) 178.32(3), P(1)–Ru–Cl(2) 94.27(3), Cl(1)–Ru–Cl(2) 88.90(3).
48 Selected bond lengths and angles of *cis*-[$RuCl_2$(dppp)(bipy)] showing the atom labelling and 30% probability ellipsoids. Bond lengths (Å): Ru(1)–N(11) 2.100(8), Ru(1)–N(12) 2.117(9), Ru(1)–P(2) 2.280(3), Ru(1)–P(1) 2.313(3), Ru(1)–Cl(11) 2.426(3), Ru(1)–Cl(12) 2.476(3). Bond angles (°): N(11)–Ru(1)–N(12) 77.3(4), N(11)–Ru(1)–P(2) 97.9(2), N(12)–Ru(1)–P(2) 92.0(2), N(11)–Ru(1)–P(1) 105.0(3), N(12)–Ru(1)–P(1) 174.3(2), P(2)–Ru(1)–P(1) 92.85(10), N(11)–Ru(1)–Cl(11) 170.2(3), N(12)–Ru(1)–Cl(11) 93.2(3), P(2)–Ru(1)–Cl(11) 84.70(10), P(1)–Ru(1)–Cl(11) 84.29(10), N(11)–Ru(1)–Cl(12) 84.1(2), N(12)–Ru(1)–Cl(12) 82.6(2), P(2)–Ru(1)–Cl(12) 173.79(11), P(1)–Ru(1)–Cl(12) 92.33(10), Cl(11)–Ru(1)–Cl(12) 92.40(9). The data of the left structure see ESI.†
49 Selected bond lengths and angles of [RuCl(dppb)(bipy)(CH_3OH)]$^+$ showing the atom labeling and 30% probability ellipsoids. Bond lengths (Å): Ru(1)–N(1) 2.083(3), Ru(1)–N(2) 2.134(3), Ru(1)–P(1) 2.2816(11), Ru(1)–P(2) 2.3381(10), Ru(1)–Cl(1) 2.4198(10), Ru(1)–O(1s) 2.249(3), O(1s)–C(1s) 1.437(6). Bond angles (°): N(1)–Ru(1)–N(2) 78.22(12), N(1)–Ru(1)–O(1s) 82.11(11), N(2)–Ru(1)–O(1s) 81.31(11), N(1)–Ru(1)–P(1)105.60(9), N(2)–Ru(1)–P(1) 90.68(9), O(1s)–Ru(1)–P(1) 167.62(8), N(1)–Ru(1)–P(2) 100.07(9), N(2)–Ru(1)–P(2) 175.09(9), O(1s)–Ru(1)–P(2) 93.91(8), P(1)–Ru(1)–P(2) 94.23(4), N(1)–Ru(1)–Cl(1) 163.42(9), N(2)–Ru(1)–Cl(1) 91.95(9), O(1s)–Ru(1)–Cl(1) 83.24(8), P(1)–Ru(1)–Cl(1) 87.64(4), P(2)–Ru(1)–Cl(1) 88.61(4).
50 Marvin was used for drawing and displaying chemical structures and reactions, *chemAxon, Marvin 15.2.9.0*, 2015, http://www.chemaxon.com.
51 M. C. R. Monteiro, F. B. Nascimento, E. M. A. Valle, J. Ellena, E. E. Castellano, A. A. Batista and S. P. Machado, *J. Braz. Chem. Soc.*, 2010, **21**(10), 1992.
52 H. Wei, J. Yin and E. Wang, *Anal. Chem.*, 2008, **80**, 5635.
53 A. N. Shipway, M. Lahav, R. Gabai and I. Willner, *Langmuir*, 2000, **16**, 8789.
54 M. Lahav, A. N. Shipway and I. Willner, *J. Chem. Soc., Perkin Trans. 1*, 1999, **2**, 1925.
55 Y. Yang, S. Matsubara, M. Nagomi and J. Shi, *Mater. Sci. Eng., B*, 2007, **140**, 172.
56 H. E. Toma, V. M. Zamarion, S. H. Toma and K. Araki, *J. Braz. Chem. Soc.*, 2010, **21**, 1158.
57 C. S. Weisbecker, M. V. Merritt and G. M. Whitesides, *Langmuir*, 1996, **12**, 3763.
58 M. G. Bellino, E. J. Calvo and G. Gordillo, *Phys. Chem. Chem. Phys.*, 2006, **6**, 424.
59 G. Von Poelhsitz, A. L. Bogado, L. M. Lião, A. G. Ferreira, E. E. Castellano, J. Ellena and A. A. Bastista, *Polyhedron*, 2010, **29**, 280.
60 M. J. Frisch, G. W. Trucks, H. B. Schlegel, G. E. Scuseria, M. A. Robb, J. R. Cheeseman, G. Scalmani, V. Barone, B. Mennucci, G. A. Petersson, H. Nakatsuji, M. Caricato, X. Li, H. P. Hratchian, A. F. Izmaylov, J. Bloino, G. Zheng, J. L. Sonnenberg, M. Hada, M. Ehara, K. Toyota, R. Fukuda, J. Hasegawa, M. Ishida, T. Nakajima, Y. Honda, O. Kitao, H. Nakai, T. Vreven, J. A. Montgomery Jr, J. E. Peralta, F. Ogliaro, M. Bearpark, J. J. Heyd, E. Brothers, K. N. Kudin, V. N. Staroverov, T. Keith, R. Kobayashi, J. Normand, K. Raghavachari, A. Rendell, J. C. Burant, S. S. Iyengar, J. Tomasi, M. Cossi, N. Rega, J. M. Millam, M. Klene, J. E. Knox, J. B. Cross, V. Bakken, C. Adamo, J. Jaramillo, R. Gomperts, R. E. Stratmann, O. Yazyev, A. J. Austin, R. Cammi, C. Pomelli, J. W. Ochterski, R. L. Martin, K. Morokuma, V. G. Zakrzewski, G. A. Voth, P. Salvador, J. J. Dannenberg, S. Dapprich, A. D. Daniels, O. Farkas, J. B. Foresman, J. V. Ortiz, J. Cioslowski and D. J. Fox, *Gaussian 09, Revision B.01*, Gaussian, Inc., Wallingford CT, 2010.
61 A. D. Becke, *J. Chem. Phys.*, 1993, **98**, 5648.
62 C. Lee, W. Yang and R. G. Parr, *Phys. Rev. B: Condens. Matter Mater. Phys.*, 1988, **37**, 785.
63 Enraf-Nonius, *Collect*, Nonius BV, Delft, The Netherlands, 1997-2000.
64 Z. Otwinowski and W. Minor, HKL Denzo and Scalepack, in *Methods in Enzymology*, ed. C. W. Carter Jr and R. M. Sweet, Academic Press, New York, 1997, vol. 276, pp. 307–326.
65 G. M. Sheldrick, *Acta Crystallogr., Sect. A: Found. Crystallogr.*, 2008, **64**, 112.
66 P. Coppens, L. Leiserowitz and D. Rabinovich, *Acta Crystallogr.*, 1965, 1035.
67 G. Frens, *Nature (London), Phys. Sci.*, 1973, **241**, 20.
68 M. B. Egorova, A. V. Dobrachenkc and A. M. Popov, *Koord. Khim.*, 1987, **13**, 541.